Bioorganic Chemistry 85 (2019) 386–398

Contents lists available at ScienceDirect

Bioorganic Chemistry

journal homepage: www.elsevier.com/locate/bioorg

Studies on lysozyme modifications induced by substituted *p*-benzoquinones

Jisook Kim*, Charles A. Thomas, Jacob M. Ewald, Neethu M. Kurien, Mary E. Booker, Hendrik J. Greve, Titus V. Albu*

Department of Chemistry and Physics, University of Tennessee at Chattanooga, Chattanooga, TN 37403, USA

ARTICLE INFO

Keywords:
Benzoquinone
Lysozyme
Protein aggregation

ABSTRACT

Protein misfolding can facilitate a protein damaging process and makes it susceptible to a series of events such as unfolding, adduct formation, oligomerization, or aggregation. Loss of a protein's native structure may result in its biological malfunction and/or cellular toxicity that could cause associated diseases. Several factors were identified for causing structural changes of a protein, however quinone-induced protein modifications received very little attention whether for amyloidal or non-amyloidal proteins. In this paper, we report our investigation on lysozyme modifications upon treatment with selected benzoquinones (BQs), utilizing fluorescence spectroscopy including anisotropy determination, UV–Vis spectroscopy, and SDS-PAGE. Lysozyme was reacted with substituted BQs in order to examine substituent effects on protein modifications. In addition, we evaluated lysozyme modifications induced by 1,4-benzoquinone in concentration-, pH-, temperature-, and time-dependent studies. Our study shows that all BQs can readily modify lysozyme in a complex manner through adduct formation, oligomerization, polymeric aggregation, and/or fibrilization. Electrochemical properties of selected BQs were monitored using cyclic voltammetry in phosphate buffered aqueous solution, and it was found that quinone reduction potentials correlate well with their reactivity trend toward lysozyme.

1. Introduction

For many eukaryotes and prokaryotes, proteins' integrity and their biological functions rely greatly on their structures, with exceptions on intrinsically disordered proteins which are known to be relatively unstructured [1–5]. It is well-known that the free energy difference between the folded and the unfolded form of a protein is small enough to allow a protein to undergo a reversible change in a conformational or structural equilibrium in order to interact with substrates or other biological molecules [2,5–7]. This reversible equilibrium or the subtle balance between the fully folded form in a native state and the partially unfolded form of a protein can be affected by various factors such as pH/temperature changes, denaturing chemicals, and mutagenic sources available in the surrounding setting [2,8–13]. In a healthy cell, the reversible balance of proteins is known to be regulated by two main pathways: (i) chaperones which refold partially-misfolded proteins and (ii) proteasomes which degrade damaged proteins [1,14–16]. When a stress factor dictates the structural stability of a protein, it could lead to formation of a potentially toxic protein such as a covalently modified protein, an oligomer precursor, disordered aggregates, and/or ordered aggregates. Such cases have been observed with amyloidal proteins that are known to associate with degenerative diseases such as Alzheimer's, Parkinson's, and hereditary lysozyme amyloidosis [2,3,5,17–19].

It was revealed that the formation of insoluble toxic proteins requires that a protein undergoes conformational/structural changes to form an initiating precursor, whether in a monomeric or an oligomeric form [2,3,5,17,18,20,21]. However, only few studies were dedicated to identifying the contributing factors that would lead to the formation of toxic proteins in their non-native states. In this regard, we explored lysozyme (LYZ) modifications induced by selected benzoquinones (BQs) under various conditions. Recently, interest on BQs and their biological roles increased since BQs are available ubiquitously in the environment as free quinones, protein cofactors, and the metabolites of polycyclic aromatic hydrocarbons [22–25]. BQs are expected to be reactive due to their redox ability and the existence of two carbonyl groups on the cyclic ring [22,23]. Previously, we reported the nature of ribonuclease

Abbreviations: LYZ, lysozyme; RQ, reduced quinone; BQ, benzoquinone; PBQ, 1,4-benzoquinone; HQ, hydroquinone; CBQ, 2-chloro-1,4-benzoquinone; FBQ, 2-phenyl-1,4-benzoquinone; TBQ, 2,3,5,6-tetrachloro-1,4-benzoquinone; MBQ, 2-methyl-1,4-benzoquinone; MM, molecular mass; NIFI, normalized integrated fluorescence intensity; A_x, absorbance at x nm; SA, solvent accessibility; RE, reference electrode; WE, working electrode; $E_{1/2}$, apparent half-wave potential; I_{pc}, cathodic peak current; I_{pa}, anodic peak current

* Corresponding authors.
E-mail addresses: jisook-kim@utc.edu (J. Kim), titus-albu@utc.edu (T.V. Albu).

https://doi.org/10.1016/j.bioorg.2019.01.018
Received 23 October 2018; Received in revised form 3 January 2019; Accepted 8 January 2019
Available online 14 January 2019
0045-2068/

A (RNase) modifications induced by 1,4-benzoquinone (PBQ), 2-methyl-1,4-benzoquinone (MBQ), and 2-chloro-1,4-benzoquinone (CBQ) utilizing SDS-PAGE, fluorescence spectroscopy, and LC-MS analysis [26–28]. In this previous work, we demonstrated that the selected BQs can modify RNase in a complex manner through a combination of adduct formation, oligomerization, and/or polymerization/aggregation. We also revealed that BQ substituent effects played an important role in RNase modifications [26–28]. Since RNase is a non-amyloidal protein, it was our next interest to extend our investigation to an amyloidal protein and to examine the nature of BQ-induced protein modifications. Quinone-induced protein modifications received little attention, in particular for amyloidal proteins. Amyloidal proteins are known for being responsible for several diseases once a protein undergoes a series of misfolding processes leading to defective structures, followed by protein aggregation or fibrillogenesis [2,3,17,18,21,29]. However, many details remain to be investigated in terms of the nature of modifications and the factors contributing to these modifications. LYZ, an amyloidal protein, was chosen for the current study because: (i) its native form is relatively stable and the structural information is available, (ii) only two tryptophan residues (W) out of the total of six W are known to be mainly responsible for the fluorescence emission [30–32], which simplify fluorescence investigation of protein modifications, and (iii) it has already been used in several other studies focusing on protein modifications related to aggregation, whether occurring in an ordered or in a partially-ordered manner [19,21,33–35].

As shown in the proposed mechanism (Fig. 1), BQs may modify a target protein in various ways which can be influenced by redox cycling of BQs and the attached substituents on the ring. The outcomes of BQs' action on a target protein can be complex, including adduct formation (path A), oligomer formation whether through noncovalent interactions (path B) or through cross-linkage (path E), lysine oxidation (path C), and oxidative damage (path D). Then, the formed oligomers can serve as precursors for formation of polymers or insoluble plaques.

In this paper, we discuss LYZ modifications induced by PBQ and other selected BQs using fluorescence spectroscopy, anisotropy, UV–Vis spectroscopy, and SDS-PAGE. We evaluated BQ substituent effects on LYZ modifications by treating LYZ with PBQ, MBQ, CBQ, 2-phenyl-1,4-benzoquinone (FBQ), and 2,3,5,6-tetrachloro-1,4-benzoquinone (TBQ), respectively. In addition, we carried out fluorescence and anisotropy determinations of LYZ modified by the presence of PBQ in a concentration-, pH-, temperature-, and time-dependent manner, respectively. Separately, we examined the redox behaviors of selected BQs in phosphate buffered aqueous solution using cyclic voltammetry (CV) in an effort to correlate quinone modification efficiency with their reduction potential trend. This study offers better insight on understanding the intricate nature of quinone-induced protein modifications of amyloidal proteins, using LYZ as an amyloidal model protein.

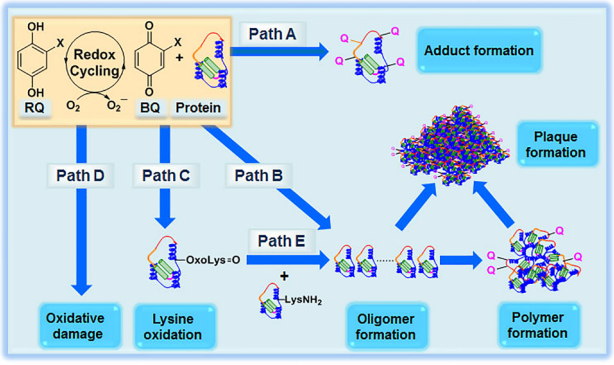

Fig. 1. Proposed modification mechanism of a protein induced by quinones. BQ, benzoquinone in an oxidized form; RQ, benzoquinone in a reduced form; Q, a quinone derivative covalently linked to the protein target.

2. Materials and methods

All chemicals were purchased from Fisher and were of reagent grade unless specified otherwise. The water used in the study was deionized water (dI-water) purified by a Millipore system (Milli-Q water). LYZ was purchased from Sigma. Electrophoresis units for minigels were purchased from Fisher. Dialysis was carried out using a 10-mL Float-A-Lyzer with a molecular weight (MW) cutoff of 3.5 kDa, which was purchased from Spectrum Laboratories. For CV experiments, ceramic patterned Pt electrodes (RRPE2001PT-6) and a reference electrode (RRPEAGCL) were purchase from Pine Research Instrumentation.

2.1. LYZ modifications detected by fluorescence spectroscopy

Fluorescence spectra and anisotropy values were obtained at 37 °C using a Horiba Jobin Yvon Fluorolog-3 spectrophotometer with a fluorescence polarization accessory and a full-spectrum, xenon-source lamp. The samples were recorded in a 1 cm × 1 cm quartz cuvette using an excitation wavelength of 280 nm. All fluorescence spectra were recorded over the 290–550 nm range in increments of 1 nm, with a band pass of 2 nm for both excitation and emission, and were intensity corrected. The unmodified and modified LYZ samples obtained post-dialysis were recorded with an integration time of 0.2 s, while the spectra of LYZ-BQ reaction mixtures were recorded with an integration time of 0.1 s. The spectra of the unmodified and the post-dialysis LYZ were normalized in the 500–550 nm range, where the protein fluorescence is negligible. The anisotropy values were determined with a band pass of 5 nm for both excitation and emission and with an integration time of 5 s.

All fluorescence studies were carried out in a 50. mM phosphate buffer solution. The pH of the solution was 7.0 except for the pH dependence studies where pH values were set at 6.0 and 8.0, respectively. The concentration of LYZ in the reaction mixtures was always 0.010 mM and was obtained by transferring aliquots of a LYZ stock solution. The BQ concentration was 0.050 mM (for a [BQ]:[LYZ] ratio of 5:1) for most studies, however other concentrations were used as well. A fresh BQ stock solution was prepared for each incubation and was used immediately after a 10 min sonication. For most studies, the fresh PBQ stock solution was prepared by dissolving PBQ in 50 mM phosphate buffer, except for the study of various BQs in which, due to solubility issues of some BQs, a solution mixture of phosphate buffer:-methanol (90:10 by volume) was used. The reaction was initiated by adding the appropriate volume (always less than 100 µL) of fresh BQ solution to a solution containing LYZ that was equilibrated at 37 °C in the temperature-controlled cell holder of the fluorimeter for 15 min, except for temperature-dependent study in which 27 °C and 24 °C were employed. The LYZ modifications in the reaction mixture were monitored every 1 h for 24 h. These hourly scans of the reaction mixture are complex because the reaction mixture contains both modified and unmodified protein as well as BQs and BQ metabolites and are not presented in this study.

Following the 24-h fluorescence monitoring, the reaction mixture was dialyzed against phosphate buffer (50 mM, pH same as the reaction mixture, 4 × 1 L per 3 mL sample) at 4 °C for 24 h. Control LYZ was subjected to the same procedure except the addition of BQ.

2.2. LYZ modifications detected by UV–Vis spectroscopy

UV–Vis spectra were obtained in a 1 cm × 1 cm quartz cuvette using a Shimadzu Biospec-1601 spectrophotometer and UV Probe 2.3 Software with a jacketed (temperature controlled) cell compartment to maintain the physiological temperature. The samples used in UV–Vis analysis were the same samples as described in the fluorescence analysis.

2.3. LYZ modifications detected by SDS-PAGE

Aliquots of LYZ stock solutions were diluted to have a final concentration of 0.10 mM LYZ and treated with each BQ (3.0 mM) in phosphate buffer (50 mM, pH 7.0), unless otherwise specified. Then, each solution was incubated at 37 °C at varied incubation time intervals, followed by immediate cooling at 0 °C to stop further protein modifications. For the pH-dependent experiments, LYZ was incubated with PBQ in 50 mM phosphate buffer at pH 6.0 and 8.0, respectively. For the temperature-dependent experiments, LYZ was incubated with PBQ under pH 7.0 at 27 and 42 °C, respectively.

For the SDS-PAGE analysis of modified LYZ, all proteins were separated on a 10% SDS-PAGE gel except the concentration dependent experiments for PBQ-treated LYZ which were separated on a 12% SDS-PAGE gel, according to the method of Laemmli [36]. Electrophoresis was performed for 2.5 h at 100 V and 30 mA per gel. Pierce Blue Prestained Protein Molecular Weight Marker Mix (Cat. # 26681) was used as a reference to determine molecular mass (MM) of protein bands. Protein bands were visualized by staining the gels with 0.1% coomassie brilliant blue G-250 blue. MM of each protein band was determined by plotting the mobility (*i.e.* represented in the distance each band traveled) against the logarithm of the proteins' MM using the Protein Molecular Weight Marker [37]. The stained gel images were submitted to quantitation using ImageJ Software to compare the distribution of monomer, dimer, trimer, and/or smearing band upon modification. The intensity values of each band corresponding to the distribution is listed under Supplementary Material section.

2.4. LYZ structure modeling and solvent accessibility scoring

The structure of LYZ was generated using the LYZ sequence obtained from the protein data bank (PDB ID: 5K2K) and viewed with the DeepView/Swiss-PdbViewer v4.1.0 [38] available at the Swiss-Prot server [39]. In order to predict the solvent accessibility of amino acid residues in LYZ, we submitted the LYZ sequence in the FASTA format to the I-TASSER on-line platform [40]. Then, a LYZ solvent accessibility scale plot was constructed with the solvent accessibility scale on y-axis and the amino acid residue number on x-axis, where the scale 9 is for a highly exposed residue and 0 is for a highly buried residue.

2.5. CV of selected BQs in phosphate buffer

CV experiments were performed with a Pine Research Intrumentation potentiostate with portable USB Wavenow equipped with a ceramic patterned Pt electrode. A Ag/AgCl electrode was used as a reference electrode (RE) for all CV measurements. Solutions were prepared at 3.0 mM for MBQ, PBQ, and CBQ in phosphate buffer (50 mM, pH 7.0) or at 1.0 mM for FBQ and TBQ due to solubility issues. The solutions above were purged with argon for 5 min and the RE was equilibrated in the buffer solution for 60 s prior to each measurement at a scan rate of 50 mV/s. For PBQ, additional measurements were carried out at scan rates of 10, 25, 75, and 100 mV/s, respectively, with 3.0 mM PBQ in phosphate buffer (50 mM, pH 7.0) at room temperature.

2.6. Reactions of LYZ and RNase with PBQ under higher-concentration conditions

To a solution of each protein (0.050 mM) in phosphate buffer (50 mM, pH 7.0) equilibrated at 37 °C, was added an aliquot of freshly prepared PBQ stock solution to achieve a final PBQ concentration of 1.5 mM. Then, each solution was scanned under fluorescence spectroscopy every hour for 24 h at 37 °C.

Table 1
Reaction conditions and properties of the modified LYZ.

Quinone	[BQ]:[LYZ][a]	pH	*T* (°C)	time (h)	NIFI	Anisotropy[b]	A_{346}[c]
None	0:1	7.0	37	24	100	0.064	0.00
MBQ	5:1	7.0	37	24	62	0.065	0.02
FBQ	5:1	7.0	37	24	39	0.067	0.04
PBQ[d]	5:1	7.0	37	24	46	0.062	0.08
CBQ	5:1	7.0	37	24	34	0.067	0.12
TBQ	5:1	7.0	37	24	22	0.076	0.17
None	0:1	7.0	37	24	100	0.064	0.00
PBQ	1:1	7.0	37	24	71	0.065	0.04
PBQ	5:1	7.0	37	24	43	0.068	0.09
PBQ	10:1	7.0	37	24	35	0.068	0.13
PBQ	30:1	7.0	37	24	19	0.075	0.13
None	0:1	6.0	37	24	89	0.032	0.02
PBQ	5:1	6.0	37	24	52	0.058	0.05
None	0:1	7.0	37	24	100	0.064	0.00
PBQ	5:1	7.0	37	24	43	0.068	0.09
None	0:1	8.0	37	24	87	0.065	0.01
PBQ	5:1	8.0	37	24	24	0.071	0.17
None	0:1	7.0	27	24	86	0.056	0.01
PBQ	5:1	7.0	27	24	54	0.069	0.03
None	0:1	7.0	37	24	100	0.064	0.00
PBQ	5:1	7.0	37	24	43	0.068	0.09
None	0:1	7.0	42	24	69	0.075	0.06
PBQ	5:1	7.0	42	24	32	0.092	0.12
None	0:1	7.0	37	24	100	0.064	0.00
None	0:1	7.0	37	0	109	0.065	0.00
PBQ	5:1	7.0	37	0	111	0.064	−0.01
PBQ	5:1	7.0	37	1	117	0.063	−0.01
PBQ	5:1	7.0	37	2	114	0.062	−0.01
PBQ	5:1	7.0	37	3	101	0.063	0.01
PBQ	5:1	7.0	37	24	43	0.068	0.09

[a] [LYZ] = 0.010 mM.
[b] Reported values were obtained by averaging the anisotropy values determined at 330, 340, and 350 nm.
[c] A_{346} represents the absorbance at 346 nm.
[d] To be consistent with the other quinones, the stock solution of PBQ used in this reaction was dissolved in a mixture of 50 mM phosphate buffer:-methanol = 90:10 by volume.

3. Results

3.1. Fluorescence and UV–Vis spectroscopy analysis of LYZ modifications

The LYZ modifications induced by various BQs were detected using fluorescence and UV–Vis spectroscopy, by treating LYZ (0.010 mM) with each BQ of interest (MBQ, FBQ, PBQ, CBQ, and TBQ at 0.050 mM), respectively. Additionally, we examined fluorescence behavior of modified LYZ obtained upon treatment with PBQ at various PBQ concentrations (0.010, 0.050, 0.10, and 0.30 mM at pH 7.0 and 37 °C), different pH conditions (pH 6.0, 7.0, and 8.0 at 37 °C), different incubation temperatures (27 °C, 37 °C, and 42 °C at pH 7.0), and various incubation time intervals (0, 1, 2, 3, and 24 h at pH 7.0 and 37 °C). The results of all these studies are summarized in Table 1.

All fluorescence spectra were normalized in the 500–550 nm range prior to data analysis. The fluorescence intensity was monitored using normalized integrated fluorescence intensity (NIFI) values. NIFI values were obtained by calculating the area under the curve of each fluorescence spectrum and by comparing, as a percentage, this area to the area obtained for LYZ unmodified by BQs but subjected to same reaction conditions. For data analysis, we examined two different integration ranges: the region of 300–400 nm encompassing the entire fluorescence area and the region of 320–360 nm focusing on the LYZ maximum fluorescence intensity. The difference between the integration results over the two regions was insignificant, therefore all the NIFI values reported here represent the data obtained over the wider range of 300–400 nm. A LYZ sample (0.010 mM) monitored for 24 h at 37 °C

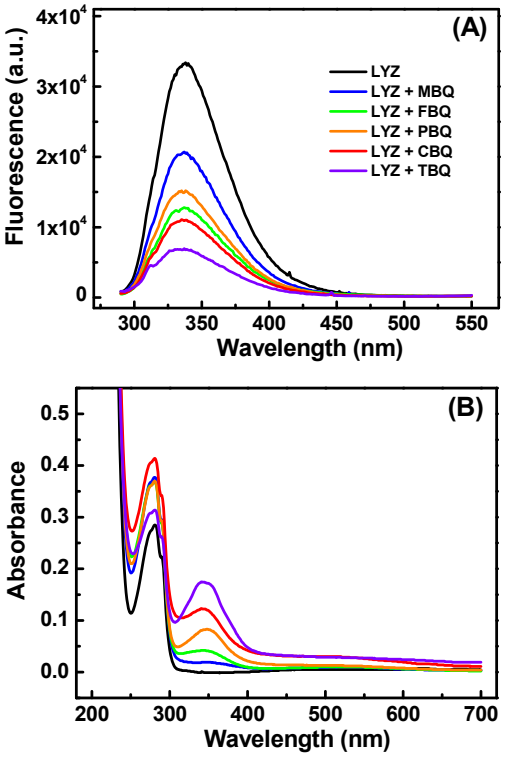

Fig. 2. (A) Fluorescence spectra and (B) UV–Vis spectra of LYZ (0.010 mM) and the post-dialysis LYZ (0.010 mM) after reacting with 0.050 mM of MBQ, FBQ, PBQ, CBQ, and TBQ, respectively, for 24 h at pH 7.0 and 37 °C.

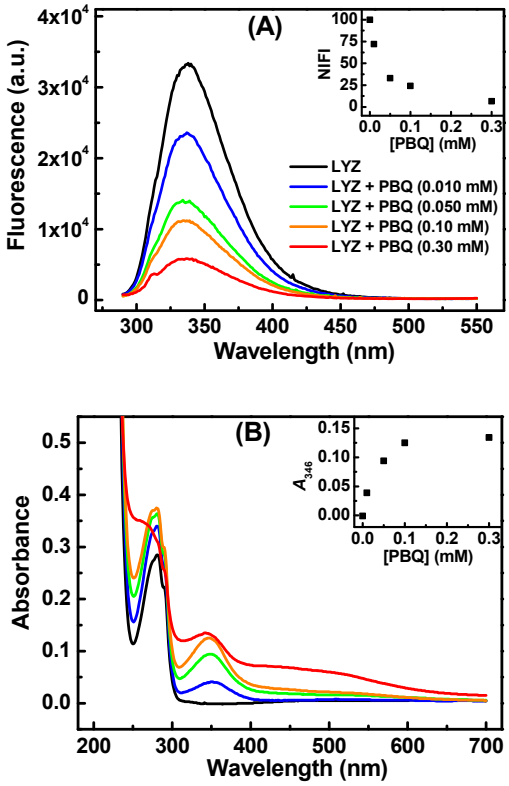

Fig. 3. (A) Fluorescence spectra and (B) UV–Vis spectra of LYZ (0.010 mM) and the post-dialysis LYZ (0.010 mM) after reacting with PBQ (0.010, 0.050, 0.10, and 0.30 mM) for 24 h at pH 7.0 and 37 °C. Graphs of NIFI and A_{346} versus PBQ concentration, respectively, are shown as insets.

in pH 7.0 followed by a 24-hour dialysis in phosphate buffer is considered to be the reference for all other LYZ samples, and it has a NIFI value of 100. Anisotropy values are also reported in Table 1. The listed anisotropy values were determined by averaging the anisotropy values measured at three different wavelengths: 330 nm, 340 nm, and 350 nm, respectively.

3.1.1. LYZ modifications induced by various BQs

In order to evaluate BQ substituent effects, LYZ (0.010 mM) was treated with MBQ, FBQ, PBQ, CBQ, and TBQ, respectively, at 0.050 mM in phosphate buffer (50. mM, pH 7.0) for 24 h at 37 °C. The reactions were allowed to undergo for 24 h while being monitored every 1 h under fluorescence spectroscopy. Then, dialysis against phosphate buffer (50. mM, pH 7.0) was performed for an additional 24 h to remove the excess unbound small molecules such as BQ and its metabolites that might interfere with protein fluorescence or UV–Vis spectrum. These post-dialysis samples of LYZ or modified LYZ, denoted as LYZ + BQ, were characterized by fluorescence spectroscopy including anisotropy determination and UV–Vis spectroscopy. Fig. 2A and B illustrates the fluorescence and UV–Vis spectra, respectively, of LYZ and LYZ + BQ samples obtained as described above.

Fig. 2A shows that there was a decrease in fluorescence intensity of LYZ + BQ compared to control LYZ. LYZ + MBQ exhibited the smallest decrease in fluorescence intensity, while LYZ + TBQ exhibited the largest decrease in fluorescence intensity. The rank order of BQ efficiency of inducing decrease in fluorescence intensity is MBQ < PBQ < FBQ < CBQ < TBQ, with TBQ being the most efficient BQ in modifying LYZ. To further quantify the degree of modification of LYZ induced by BQ substituent effects, NIFI values were compared to the NIFI of unmodified LYZ (0.010 mM) as the reference (*i.e.*, NIFI value of 100). As presented in Table 1, NIFI value typically decreased as each substituent becomes more electron withdrawing. For example, NIFI values for LYZ treated with each BQ were 62 for LYZ + MBQ, 39 for LYZ + FBQ, 46 for LYZ + PBQ, 34 for LYZ + CBQ, and 22 for LYZ + TBQ, respectively. It is interesting to note that anisotropy values reported in Table 1 for the modified LYZ tend to increase as the fluorescence intensity decreases indicating also a more significant modification of LYZ, most likely associated with an increase in protein size through oligomerization. A correlation graph between anisotropy and NIFI is included in the Supplementary Material.

Fig. 2B shows that control LYZ exhibited the maximum absorption at 280 nm, while LYZ + BQ samples exhibited an additional distinctive chromophore ranging in the 300 to 400 nm region. The absorbance values at 346 nm (A_{346}) were 0.0 for LYZ, 0.02 for LYZ + MBQ, 0.04 for LYZ + FBQ, 0.08 for LYZ + PBQ, 0.12 for LYZ + CBQ, and 0.17 for LYZ + TBQ, respectively. An increase in the A_{346} for all BQs was observed in conjunction with a decrease in NIFI compared to control LYZ.

3.1.2. LYZ modifications induced by PBQ at various concentrations

For PBQ concentration-dependent LYZ modification study, LYZ (0.010 mM) was treated with PBQ at various concentrations at 0.010, 0.050, 0.10, and 0.30 mM, respectively, in phosphate buffer (50. mM, pH 7.0) at 37 °C for 24 h. Each reaction was monitored using fluorescence for 24 h, followed by 24 h dialysis and the final spectroscopic analysis. Fig. 3 shows the fluorescence and UV–Vis spectra of control LYZ and LYZ modified by PBQ at various concentrations. As presented in the Fig. 3A, the fluorescence intensity decreased as PBQ concentration increased from 0.010 mM to 0.30 mM. NIFI values (Table 1) were found to be 100 at 0 mM, 71 at 0.010 mM, 43 at 0.050 mM, 35 at 0.10 mM, and 19 at 0.30 mM of PBQ, respectively. The NIFI show that the increase in PBQ concentration resulted in the decrease of LYZ fluorescence emission. As PBQ concentration increased from 0.010 mM to 0.30 mM, the absorbance in 300–400 nm range increased (Fig. 3B). The A_{346} values with increasing PBQ concentration are 0.00 at 0 mM, 0.04 at 0.010 mM, 0.09 at 0.050 mM, 0.13 at 0.10 mM, and 0.13 at 0.30 mM of PBQ, respectively.

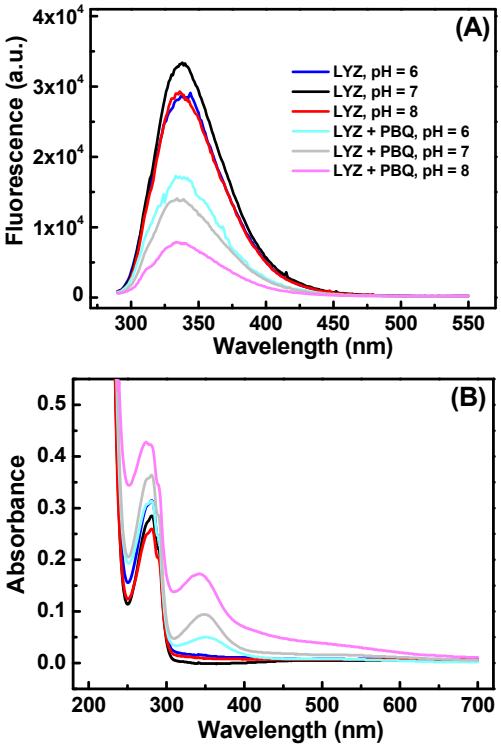

Fig. 4. (A) Fluorescence spectra and (B) UV–Vis spectra of LYZ (0.010 mM) and the post-dialysis LYZ (0.010 mM) after reacting with PBQ (0.050 mM) at pH 6.0, 7.0, and 8.0 for 24 h at 37 °C.

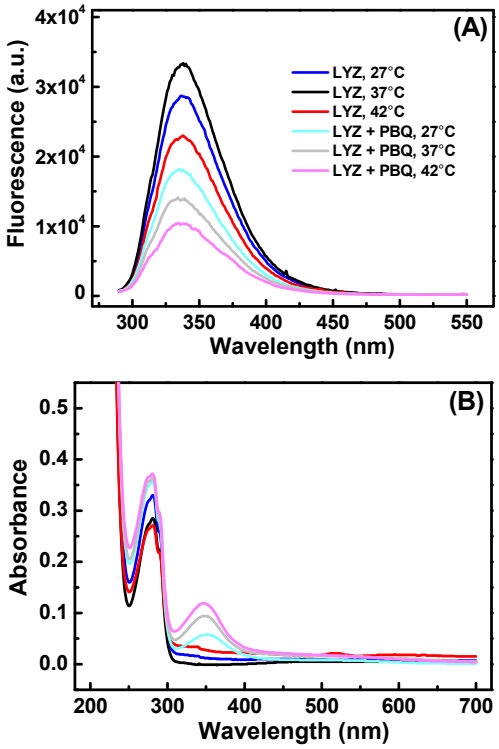

Fig. 5. (A) Fluorescence spectra and (B) UV–Vis spectra of LYZ (0.010 mM) and the post-dialysis LYZ (0.010 mM) after reacting with PBQ (0.050 mM) at 27 °C, 37 °C, and 42 °C for 24 h at pH 7.0.

3.1.3. LYZ modifications induced by PBQ at different pH values

For pH-dependent LYZ modification study, LYZ (0.010 mM) was incubated for 24 h in the absence and the presence of PBQ (0.050 mM) at pH 6.0, 7.0, and 8.0, respectively. All reactions were performed in 50 mM phosphate solutions at 37 °C. Following the 24 h incubation and 24 h dialysis, the samples denoted LYZ or LYZ + PBQ, respectively, were characterized by fluorescence and UV–Vis spectroscopy. Fig. 4 shows the fluorescence and UV–Vis spectra of control LYZ and LYZ modified by PBQ at different pH conditions. As presented in Fig. 4A, the fluorescence spectra of LYZ at different pH conditions, in the absence of PBQ are consistent with the previously reported studies [41,42]. Fig. 4A also shows the fluorescence intensity of LYZ + PBQ decreased as pH increased from 6.0 to 8.0, rather than having a maximum at pH 7.0 as seen for control LYZ. Even though the fluorescence of unmodified LYZ also varies with pH, NIFI values for LYZ + PBQ of 52 at pH 6.0, 43 at pH 7.0, and 24 at 8.0, respectively, show that the increase of solution pH results in a decrease the fluorescence intensity of modified LYZ, consistent with enhanced protein modifications. Fig. 4B shows that the absorbance in the 300–400 nm region for LYZ + PBQ increased as the solution pH increased. As presented in Table 1, A_{346} values of LYZ + PBQ were 0.05 at pH 6.0, 0.09 at pH 7.0, and 0.17 at pH 8.0, respectively.

3.1.4. LYZ modifications induced by PBQ at different temperatures

For temperature-dependent LYZ modification study, LYZ (0.010 mM) was treated with PBQ (0.050 mM) in phosphate buffer (50. mM, pH 7.0) and allowed to react at 27 °C, 37 °C, and 42 °C, respectively, while being monitored by fluorescence spectroscopy for 24 h. Following the 24 h dialysis, the final spectroscopic analysis of control LYZ and LYZ + PBQ was carried out at 37 °C. Fig. 5 shows the fluorescence and UV–Vis spectra of control LYZ and LYZ modified by PBQ at different temperatures. As seen in Fig. 5A, the fluorescence intensity for LYZ + PBQ decreased as temperature increased from 27 °C to 42 °C. NIFI values of 54 at 27 °C, 43 at 37 °C, and 32 at 42 °C, respectively, show that the increase of reaction temperature causes a decrease in the fluorescence emission due to more LYZ modifications by PBQ at higher temperatures. Fig. 5B shows the UV–Vis spectral feature of LYZ + PBQ at 27 °C, 37 °C, and 42 °C, respectively. The absorbance in the 300–400 nm region increased as the temperature of the reaction increased. Table 1 presents A_{346} values of 0.03 at 27 °C, 0.09 at 37 °C, and 0.12 at 42 °C, respectively, for LYZ + PBQ.

3.1.5. LYZ modifications induced by PBQ over various incubation times

For time-dependent LYZ modification study, LYZ (0.010 mM) was treated with PBQ (0.050 mM) in phosphate buffer (50 mM, pH 7.0) at 37 °C and allowed to react while being monitored using fluorescence for 0, 1, 2, 3, and 24 h. Following each incubation, dialysis was performed for 24 h prior to submission to a final spectroscopic measurement of modified LYZ. Fig. 6 illustrates the fluorescence and UV–Vis spectra of control LYZ (24 h monitoring at 37 °C) and post-dialysis LYZ + PBQ for various reaction times. Both Fig. 6A and the NIFI values in Table 1 shows that the fluorescence intensity of LYZ + PBQ samples for the reactions under the shorter incubation intervals was higher than those of control LYZ at 0 h (not shown in the figure) as well as control LYZ at 24 h. NIFI values in Table 1 are 109 for control LYZ at 0 h, 100 for control LYZ at 24 h, 111 for LYZ + PBQ at 0 h, 117 for LYZ + PBQ at 1 h, 114 for LYZ + PBQ at 2 h, 101 for LYZ + PBQ at 3 h, and 43 for LYZ + PBQ at 24 h. Fig. 6B also shows that, as the incubation time increased from 1 to 24 h, the absorbance at 346 nm increased. For example, A_{346} values were found to be −0.01 at 1 and 2 h, 0.01 at 3 h, and 0.09 at 24 h, respectively.

3.2. SDS-PAGE analysis of LYZ modifications induced by various BQs

In an effort to investigate LYZ oligomerization and polymerization induced by BQ substituent effects, SDS-PAGE experiments were performed. Typical SDS-PAGE analysis was carried out by incubating LYZ (0.10 mM) and each BQ (3.0 mM) up to 24 h in phosphate buffer

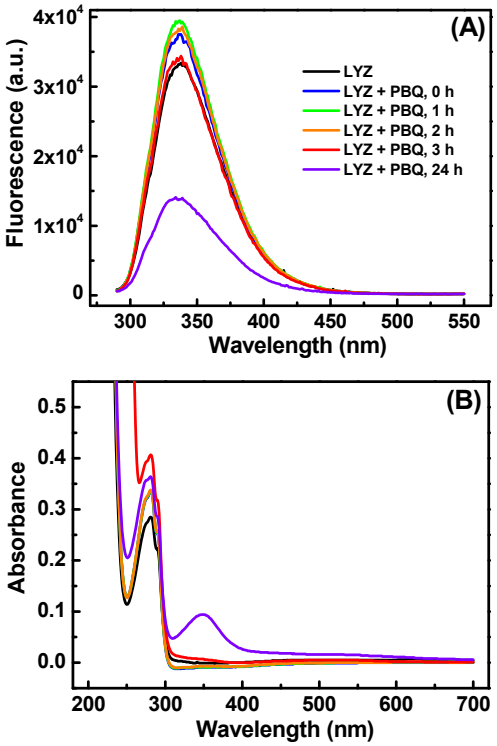

Fig. 6. (A) Fluorescence spectra and (B) UV–Vis spectra of LYZ (0.010 mM) and the post-dialysis LYZ (0.010 mM) after reacting with PBQ (0.050 mM) for 0, 1, 2, 3, and 24 h at pH 7.0 and 37 °C.

(50 mM, pH 7.0) at 37 °C unless otherwise stated. Note that [LYZ] in SDS-PAGE experiments is 10-fold bigger than [LYZ] in fluorescence/UV–Vis experiments.

Fig. 7 represents the gel features of LYZ treated with selected BQs, each labelled as LYZ + MBQ (A), LYZ + FBQ (B), LYZ + PBQ (C), LYZ + CBQ (D), and LYZ + TBQ (E), respectively. Both LYZ + MBQ and LYZ + FBQ incubations exhibited a simple gel feature with two major bands around 14 and 29 kDa as incubation time increased, except for 24 h samples where a band around 43 kDa and some smearing bands appeared (Fig. 7A/B). In contrast, incubation of LYZ with PBQ, CBQ, and TBQ resulted in the formation of multiple bands around 14, 29, and 43 kDa, respectively, together with smearing bands at the high MW region (Fig. 7C–E). The formation of smearing bands started as early as 30 min for all three PBQ, CBQ, and TBQ, with CBQ and TBQ being more efficient in smearing-induction over a span of incubation time intervals. The estimated band intensity at 29 kDa for 30 min incubation is approximately 0% for both MBQ and FBQ, 41% for PBQ, 28% for CBQ, and 30% for TBQ, respectively. The estimated band intensity at 43 kDa for 30 min incubation is approximately 0% for both MBQ and FBQ, 14% for PBQ, 15% for CBQ, and 20% for TBQ, respectively. The estimated band intensity of smearing band for 30 min incubation is approximately 9% for PBQ, 24% for CBQ, and 37% for TBQ, respectively. All these band intensities are tabulated in the Supplementary Material. The smearing bands faded out at 24 h for PBQ, CBQ, and TBQ-treated LYZ. The weakening of the smearing bands was accompanied by formation of fibrillous LYZ plaques that were insoluble in loading buffer and the plaques precipitated out of the solution.

3.3. SDS-PAGE analysis of LYZ modifications induced by PBQ

For investigating the influence of various reaction conditions, LYZ (0.10 mM) was incubated with PBQ while varying PBQ concentration (0.10, 0.50, and 1.0 mM, respectively, under pH 7.0 and 37 °C), pH conditions (pH 6.0, 7.0, and 8.0, respectively, under 3.0 mM PBQ and 37 °C), and incubation temperatures (27 °C, 37 °C, and 42 °C, respectively, under 3.0 mM PBQ and pH 7.0).

Fig. 8 shows the gel features of LYZ + PBQ where LYZ (0.10 mM) was reacted with PBQ (0.10, 0.50, and 1.0 mM) up to 24 h at pH 7.0 and 37 °C. The band formation at 29 kDa became obvious around 3 h at 0.10 mM, 30 min at 0.50 mM, and 10 min at 1.0 mM PBQ, respectively. The estimated band intensity at 29 kDa is approximately 13% for 3 h at 0.10 mM, 6% for 30 min at 0.5 mM, and 17% for 10 min at 1.0 mM PBQ, respectively. The formation of the band around 43 kDa followed a similar trend, appearing as a noticeable band at 24 h for 0.10 mM, 3 h for 0.50 mM, and 1 h for 1.0 mM PBQ, respectively, as PBQ concentration increased from 0.10 mM to 1.0 mM. The estimated band intensity at 43 kDa is approximately 7% at 24 h for 0.10 mM, 8% at 3 h for 0.50 mM, and 11% at 1 h for 1.0 mM PBQ, respectively (see Supplementary Material). For 1.0 mM PBQ-treated LYZ, fading of smearing bands with mild plaque formation was observed as incubation time increased.

Fig. 9 illustrates the gel features of LYZ + PBQ in pH 6.0, 7.0, and 8.0 upto 24 h at 37 °C, respectively. As pH increased from 6.0 to 8.0, the degree of modification intensified based on the formed bands around 29 and 43 kDa including smearing bands. The band at 29 kDa appeared as early as 30 min for all three examined pH conditions, however the band at 43 kDa appeared at 3 h for pH 6.0, 30 min for pH 7.0, and 10 min for pH 8.0. The estimated band intensity at 29 kDa for 30 min incubation is approximately 19% for pH 6.0, 37% for pH 7.0, and 28% for pH 8.0, respectively. The estimated band intensity at 43 kDa is approximately 6% at 3 h for pH 6.0, 11% at 30 min for pH 7.0, and 8% at 10 min for pH 8.0, respectively. Formation of smearing bands appeared at 24 h for pH 6.0, 60 min for pH 7.0, and 10 min for pH 8.0. The smearing feature was observed over a range of incubation time intervals for both pH 7.0 and 8.0, then it faded out at 24 h. LYZ plaque formation was observed as the smearing bands faded out.

Fig. 10 shows the gel features of LYZ + PBQ at 27 °C, 37 °C and 42 °C up to 24 h at pH 7.0, respectively. The band at 29 kDa appeared as early as 10 min for all three temperatures, however the band at 43 kDa became obvious at 1 h for 27 °C, 30 min for 37 °C, and 10 min for 42 °C. The estimated band intensity at 29 kDa for 10 min incubation is

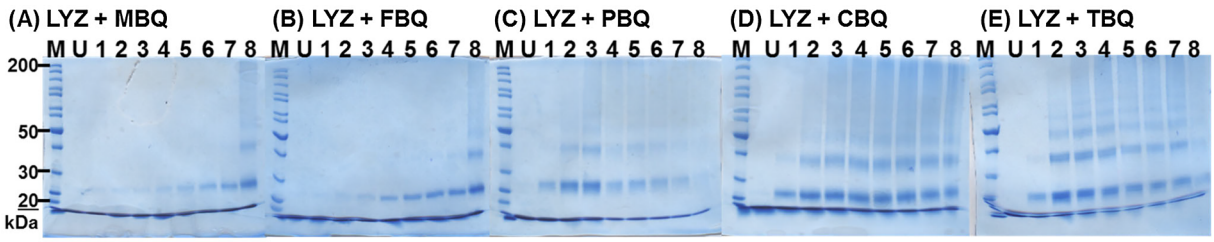

Fig. 7. SDS-PAGE of LYZ (0.10 mM) upon exposure to each quinone (3.0 mM): (A) LYZ + MBQ, (B) LYZ + FBQ, (C) LYZ + PBQ, (D) (C) LYZ + CBQ, (E) LYZ + TBQ. Reactions were carried out at pH 7.0 and 37 °C for 10, 30, 60, 120, 180, 240, 300 min, and 24 h. Each lane denotation represents MM, protein standard molecular marker; U, unmodified LYZ; 1, lane 1 for 10 min; 2, lane 2 for 30 min; 3, lane 3 for 1 h; 4, lane 4 for 2 h; 5, lane 5 for 3 h; 6, lane 6 for 4 h; 7, lane 7 for 5 h; 8, lane 8 for 24 h.

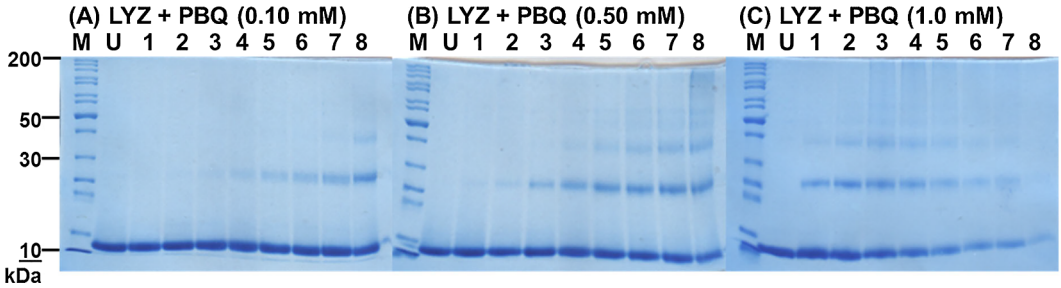

Fig. 8. SDS-PAGE of LYZ (0.10 mM) + PBQ for 24 h at pH 7.0 and 37 °C: (A) [PBQ] = 0.10 mM, (B) [PBQ] = 0.50 mM, (C) [PBQ] = 1.00 mM. Each lane denotation is same as Fig. 7.

approximately 14% for 27 °C, 27% for 37 °C, and 46% for 42 °C, respectively. The estimated band intensity at 43 kDa for 1 h incubation is approximately 8% for 27 °C, 12% for 37 °C, and 16% for 42 °C, respectively (see Supplementary Material). The smearing feature was observed as early as 2 h for 27 °C, 1 h for 37 °C, and 30 min for 42 °C. Fading of the smearing bands became obvious around 24 h for 37 °C and 42 °C and was accompanied by LYZ plaque formation.

3.4. LYZ structure modeling and solvent accessibility scoring

In an effort to better understand the roles of key amino acid residues on LYZ modifications as well as its spectroscopic behavior, we visualized the locations of lysine (*i.e.*, K; residue numbers: 1, 13, 33, 96, 97, 116), tryptophan (*i.e.*, W; residue numbers: 28, 62, 62, 108, 111, 123), and tyrosine (*i.e.*, Y; residue numbers: 20 and 23) residues in LYZ, using DeepView-SwissPDB Viewer (Fig. 11). In addition, we evaluated the solvent accessibility (SA) of all 129 amino acid residues in LYZ (Fig. 12). The SA profile was generated by the on-line format I-TASSER [40], on the scale of 0–9, where the value 0 represents a buried residue and the value 9 represents a highly exposed residue to solvent. In the rendered view, it appears that most of K residues are located at the surface of LYZ rather than being buried inside the protein, however Fig. 12A revealed that only K1 and K116 have a reasonably good solvent accessibility with the value of 7 and 5, respectively, while the averaged SA value for other four lysine's were 3. On the rendered structure (Fig. 11A), there are two subgroups of K, W, and Y residues; the first subgroup (SG1) includes K1, K13, K33, K96, K97, K116, W62, W63, and Y53 which are located at the relatively exterior of LYZ, while the second subgroup (SG2) includes Y20, Y23, W28, W108, and W111 which are in proximity to each other, and mostly located inside LYZ except K116. The rendered locations of W and Y are consistent with low SA values (< 1) except Y20, Y23, and W62 with SA values of 3. There are three hydrogen bonds between C═O of W108/NH_α of W111, C═O of Y20/NH_α of Y23, and C═O of W111/NH_α of K116, in addition to multiple hydrogen bonds present over other regions of LYZ.

Fig. 11C illustrates the zoom-in view of W and Y residues in SG2 where these residues form a pocket, having the C_α–C_α distance of 3.8 Å for W62/W63, 5.3 Å for W108/W111, 5.5 Å for Y20/Y23, 7.5 Å for W28/Y23, 10.2 Å for Y23/W111, 10.3 Å for W108/W28, and 13.3 Å for W108/W62, respectively. The N—H (indole) distances between two W residues in SG2 are 5.9 Å for W62/W63, 9.5 Å for W108/W111, 10.0 Å for W108/W28, and 12.7 Å for W108/W62, respectively. The OH_{tyr}–NH_{indole} distances between W and Y residues in SG2 are 6.9 Å for W111/Y23 and 8.7 Å for W28/Y23. The OH_{tyr}–NH_{indole} distances between W and Y residues in SG2 are 6.9 Å for W111/Y23 and 8.7 Å for W28/Y23. Finally, the OH distance between two Y residues in SG2 is 12.3 Å for W28/Y23. It is interesting to note that these distances between each pair of W/W, W/Y, and Y/Y in SG2 fall within the typical range for the Föster distances for energy transfer whether heterotransfer (Y-to-W or W-to-Y) or homotransfer (W-to-W or Y-to-Y) [43]. The location of phenylalanine was not considered since W and Y rather than phenylalanine contribute to the intrinsic fluorescence in many proteins.

3.5. CV of selected BQs in phosphate buffer

In an effort to understand how each quinone's electrochemical properties correlate to BQ's efficiency on modifying LYZ, we carried out CV experiments on selected BQs containing various substituents. For the measurements, each quinone (3.0 mM) was dissolved in phosphate buffer (50 mM, pH 7.0), except FBQ and TBQ which were set at 1.0 mM due to their solubility issue. Then, each solution was submitted to CV measurements at a specified scan rate.

Fig. 13A illustrates the key feature of a typical cyclic voltammogram of BQ, specifically for PBQ (3.0 mM) in phosphate buffer recorded at a scan rate of 50 mV/s. BQ is going through its reduction and oxidation, where the working electrode (WE) starts at high potential with respect to the RE (region I, Fig. 13A). The two arrows represent the movement of sweeping potentials from high to low and back to high values. As the system reaches the negative potential reducing BQ to the corresponding reduced quinone (RQ) due to 2 e^- transfer from WE to BQ, the cathodic current increases until BQ is consumed, resulting in the cathodic peak current (I_{pc}). Once passing I_{pc}, there is current decay as all BQ around WE is depleted (region II, Fig. 13A), therefore the detected current at WE at this point is limited by the diffusion rate of BQ in the non-Nernst diffusion layer (*i.e.*, the bulk solution [44]) and the current decays depending on time$^{-1/2}$. As the potential increases back at the region III and IV, RQ is oxidized back to BQ with the potential increase. Simultaneously, the backward potential sweep results in the anodic peak current (I_{ac}), while 2 e^- were transferred back to WE and 2 H^+ moved

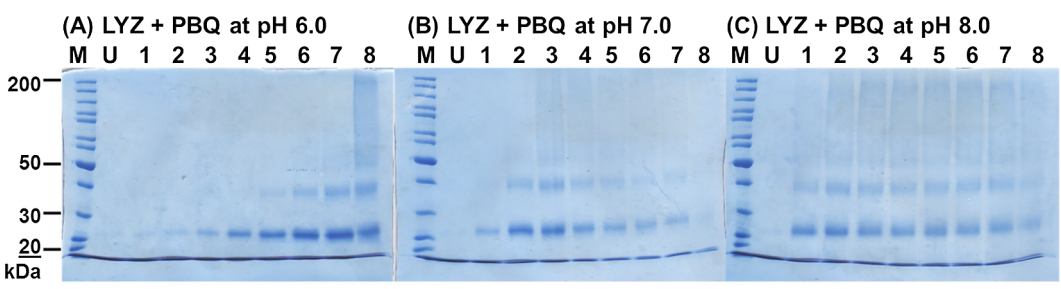

Fig. 9. SDS-PAGE of LYZ (0.10 mM) + PBQ (3.0 mM) for 24 h and 37 °C: (A) at pH 6.0, (B) at pH 7.0, (C) at pH 8.0. Each lane denotation is same as Fig. 7.

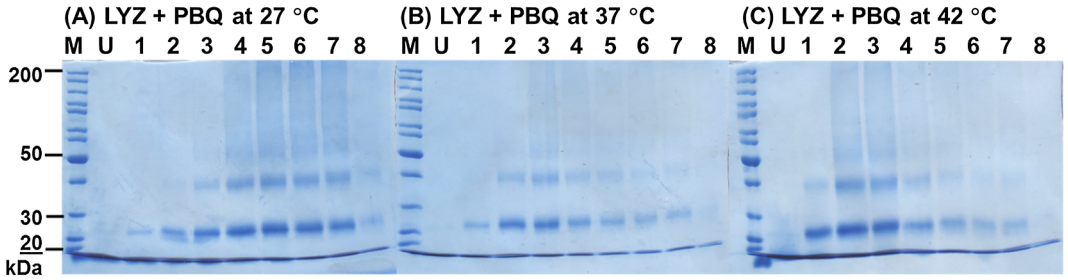

Fig. 10. SDS-PAGE of LYZ (0.10 mM) + PBQ (3.0 mM) for 24 h and pH 7.0 (A) at 27 °C, (B) at 37 °C, (C) at 42 °C. Each lane denotation is same as Fig. 7.

back to the buffer.

Fig. 13B illustrates overlaid cyclic voltammograms of MBQ, FBQ, PBQ, CBQ, and TBQ, respectively, in phosphate buffer, recorded at a scan rate of 50 mV/s. The difference value between the anodic (oxidative) peak potential (E_{pa}) and the cathodic (reductive) peak potential (E_{pc}), $\Delta E = |E_{pa} - E_{pc}|$, varied among BQs, as the substituent on each quinone varied. A CV feature of a reversible electron transfer was observed for MBQ, FBQ, PBQ, and CBQ, with a calculated apparent half-wave potential ($E_{1/2}$) of 54, 70, 83, and 98 mV vs. Ag/AgCl, respectively, while a quasi-reversible CV feature was observed for TBQ with an approximated $E_{1/2}$ value to be higher than 300 mV. The reversible feature for the four BQs except TBQ was further evaluated by examining the dependence of the peak current height (I_p) on the square root of the scan rate (ν), following Randles-Sevcik equation below (Eq. (1)) [44,45], where I_p = peak current in Ampere, n = number of electrons, R = electrode area (cm^2), C = concentration (mol/cm^3), D = diffusion coefficient (cm^2/sec), ν = scan rate (typically V/sec):

$$I_p = (2.69 \times 10^5) n^{3/2} R C D^{1/2} \nu^{1/2} \quad (1)$$

In order to determine the linearity of I_p vs. $\nu^{1/2}$ for PBQ over a range of scan rates, CV scans were collected at varied scan rates of 10, 25, 50, 75, and 100 mV/s, respectively, then, the anodic and the cathodic I_p values were plotted against $\nu^{1/2}$. Fig. 13C shows the overlaid CV scans where both I_p increased as ν increased, and Fig. 13D shows linear relationships observed for the plots of I_p vs. $\nu^{1/2}$.

4. Discussion

In our previous work, we reported BQ-induced ribonuclease A (RNase) modifications which occurred in a complex manner involving adduction formation, crosslinking, and/or polymerization [22,26,27]. To extend our investigation on the role of BQs toward proteins, we carried out the present study focusing on modifications of an amyloidal protein LYZ induced by various BQs. In addition, we investigated the effects of other factors on protein modification such as quinone concentrations, pH, and temperature when LYZ was treated with PBQ.

An important objective of the current study was to investigate if and how various BQs modify LYZ. In addition to PBQ, MBQ and FBQ were chosen as BQs with electron-donating groups, while CBQ and TBQ were chosen as BQs with electron-withdrawing groups. The presence of an electron-withdrawing substituent is expected to decrease the electron density and to make the carbon of C═O in the BQ more electrophilic, therefore more susceptible to reactions with nucleophilic amino acid residues. However, the presence of an electron-donating substituent would have the opposite effect.

The fluorescence study of LYZ modified by MBQ, FBQ, PBQ, CBQ, and TBQ, respectively, supports the idea of BQ substituent effects influencing LYZ modification. It appears that electron-donating groups on BQ caused less LYZ modification, while electron-withdrawing groups resulted in greater modification. The degree of LYZ modification was confirmed by comparing NIFI values (Table 1) of 62 for LYZ + MBQ and 22 for LYZ + TBQ as an example. As mentioned earlier, a large NIFI value represents a higher fluorescence intensity therefore less protein modification, while a low NIFI value represent a decrease in fluorescence intensity and more significant protein modifications. Overall, the rank order of NIFI values is as follows: MBQ > PBQ > FBQ > CBQ > TBQ. One exception was FBQ, with an electron-donating group, however with a NIFI lower than PBQ. It is possible that even though the modifications induced by FBQ are not as significant as those induced by PBQ, they are associated with smaller fluorescence intensity. Due to the large size of a phenyl group at the carbon-2 position, adduct formation involving FBQ would probably change the protein conformation to a greater extent than PBQ adduct formation. A lower quantum yield, therefore lower fluorescence intensity, is also possible for FBQ-induced LYZ modifications compared to PBQ-induced modifications.

UV–Vis data (Fig. 2B) confirms that absorption in the 300–400 nm region increased for LYZ modified by all five BQs under examined conditions. Control LYZ had maximum absorption at 280 nm without any significant absorption in the 300–400 nm region, while BQs absorb in this range. Since the UV–Vis spectra reported in this paper were obtained after 24 h dialysis, any unbound, free quinones or their metabolites were removed through dialysis at this stage [26–28]. Therefore, the observed absorption in the 300–400 nm region corresponds to LYZ modified by BQ being covalently bonded (*i.e.*, adduct formation), without the contribution from unbound quinones. It is interesting to point out that the A_{348} values are consistent with electronic effects of the substituent, with BQs with electron-donating substituents (MBQ and FBQ) having small A_{348} values and BQs with electron-withdrawing

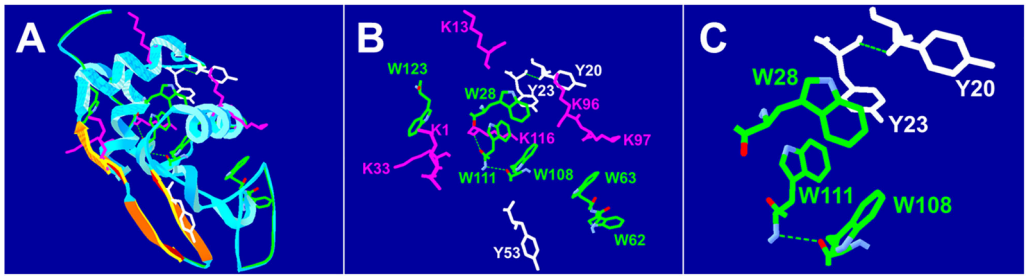

Fig. 11. Model structure of LYZ rendered by DeepView/Swiss-PdbViewer. K, lysine; W, tryptophan; Y, tyrosine. Dashed lines represent hydrogen bonds. (A) LYZ in a ribbon structure with K, Y, and W, (B) K, Y, and W in SG1 and SG2; green dotted lines represent hydrogen bonds, (C) K, Y, and W in SG2.

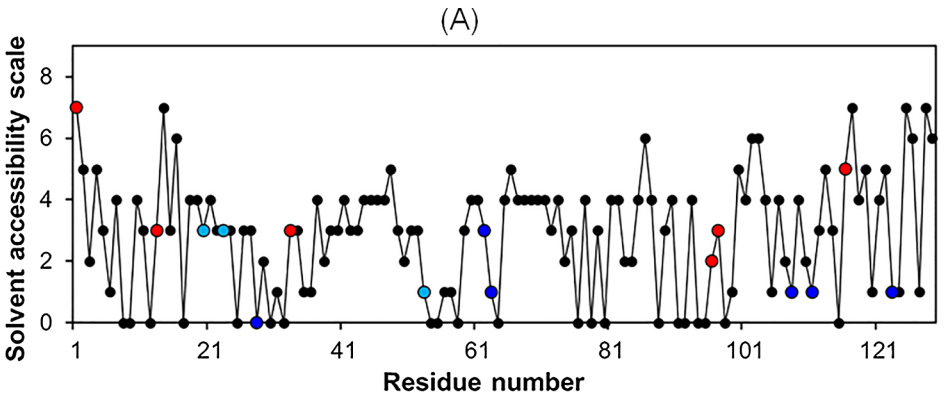

(B)

Residue 1 to 40	1 10 13 20 23 28 30 33 40 KVFGRCELAA AMKRHGLDNY RGYSLGNWVC AAKFESNFNT
Residue 41 to 90	41 50 53 60 62 63 70 80 90 QATNRNTDGS TDYGILQINS RWWCNDGRTP GSRNLCNIPC SALLSSDITA
Residue 91 to 129	91 96 97 100 108 110 111 116 120 123 129 SVNCAKKIVS DGNGMNAWVA WRNRCKGTDV QAWIRGCRL

Fig. 12. (A) Solvent accessibility scale vs. residue number of LYZ, determined by I-TASSER. Lysine marked with ●, tryptophan marked with ● and tyrosine marked with ●, where the scale 9 for a highly exposed residue and 0 for a highly buried residue, (B) LYZ sequence.

substituents (CBQ and TBQ) having larger A_{348} values.

SDS-PAGE experiments were carried out to investigate LYZ modification through aggregation, whether oligomerization or polymerization. As shown in the proposed mechanism (Fig. 1), the condensation reaction of a lysine residue in a LYZ molecule and an oxo-lysine residue in another modified LYZ is expected to lead to formation of oligomers such as dimer (29 kDa) and trimer (43 kDa), followed by further advance to polymerization. In a previous study, we reported the detection of the formed oxo-lysine by trapping it as a hydrazone analog after treating modified and post-dialyzed RNase with 2,4-dinitrophenylhydrazine [28]. Furthermore, an LC-ESI$^+$-QTOF-MS investigation on RNase control, PBQ-modified RNase, and CBQ-modified RNase revealed that RNase underwent complex modifications including adduct formation as well as oligomerization upon treatment with BQs [26]. These two findings serve as the evidence of lysine being a target for BQs in RNase, and LYZ is expected to undergo similar types of modifications. The formation of a dimer band, appearing at the slightly higher MW than the 25 kDa marker region, was observed in Fig. 7 for LYZ modified by all five BQs, as incubation time increased from 10 min (lanes 1) to 24 h (lanes 8). MBQ and FBQ, both with electron-donating substituents, exhibited lower reactivity, inducing mild level of LYZ dimerization over 10 min–5 h incubation time, followed by LYZ polymeric aggregation at 24 h. CBQ and TBQ exhibited significant reactivity toward LYZ, inducing dimerization as early as 10 min (lanes 1 for LYZ + CBQ and LYZ + TBQ, Fig. 7) and oligomerization appearing as multiple bands as early as 30 min. In case of LYZ + TBQ at 24 h (lane 8 for LYZ + TBQ), severe LYZ modifications were detected with formation of LYZ plaques which were insoluble in solubilizing buffer. This finding suggests that chemico-physical property of quinones might be one of the contributing factors for inducing plaque formation, since the plaque formation was more evident for CBQ- and TBQ-treated LYZ compared to MBQ or FBQ-treated LYZ. Also, it implies that the nature of covalently linked BQ to LYZ might play an important role in plaque formation as well as adduct formation, oligomerization, and/or polymerization.

To correlate LYZ modification with BQ substituent effects measured by BQ electrochemical properties, CV experiments were performed with MBQ, FBQ, PBQ, CBQ, and TBQ in phosphate buffer. It was found that the redox cycling of MBQ, FBQ, PBQ, and CBQ are electrochemically reversible, while TBQ exhibited quasi-reversibility. Similar to PBQ, the linearity feature of I_p vs. $\nu^{1/2}$ was observed for MBQ, FBQ, and CBQ but not TBQ (data not shown). Quinones are expected to go through redox-cycling involving 2 e^- and 2 H^+ between BQ and RQ (Eq. (2)) in buffered aqueous solution, while the cycling mechanism could be more complex in either un-buffered or aprotic solutions [46]. A large peak-to-peak separation was observed for MBQ, FBQ, PBQ, and CBQ, as the scan rate increased. This is a typical indication for a slow electron-transfer process [46]. Unlike other BQs which underwent a simple E mechanism where E represents an electron-transfer step at the electrode (Eq. (2)), TBQ appeared to exhibit a quasi-reversible feature. The CV behavior of TBQ implies that TBQ follows an EC mechanism where the first E step is followed by a C step in which a chemical reaction generates probably a dechlorinated species (Z in Eq. (3)) which is electrochemically inactive under the examined conditions in the scanned potential range [44,45,47].

$$BQ + 2e^- + 2H^+ \leftrightharpoons RQ \text{ for MBQ, FBQ, PBQ, and CBQ} \quad (2)$$

$$TBQ + 2e^- + 2H^+ \leftrightharpoons TRQ \leftrightharpoons Z \quad (3)$$

CV experiments together with the other findings suggest that the higher the BQ reduction potential given by $E_{1/2}$, the more modifications were induced in LYZ. For example, MBQ and FBQ have the $E_{1/2}$ values of 54 and 70 mV, respectively, and both were found to be less efficient in modifying LYZ based on fluorescence and SDS-PAGE data, while both CBQ and TBQ, with $E_{1/2}$ values higher than 90 mV, resulted in severe decrease in fluorescence intensity and higher level of LYZ polymerization accompanied also by visually observed plaque formation. Therefore, this correlation study shows that the electrochemical profile of BQs may serve as a marker for predicting BQs' biological activities toward protein modifications. The correlation between BQ reactivity and the electrochemical profile might provide some answers to why certain quinones could inhibit amyloidosis rather than inducing amyloidosis. For example, catechol-type flavonoids such as taxifolin and balcalein are reported as amyloidosis inhibitors [48–50]. Considering the structural difference between these flavonoids having a bigger ring and more OH groups and PBQ and the likely different electrochemical properties, it should not be surprising that these substances could have opposite effects on amyloidosis.

Another important objective of the current study was to investigate how various reaction conditions influence LYZ modifications by PBQ. As expected, by increasing the concentration of PBQ, more significant LYZ modifications are observed. As PBQ concentration increased from 0.010 mM to 0.30 mM, the fluorescence intensity of LYZ + PBQ decreased (Fig. 3A), NIFI values decreased (Table 1) and A_{346} increased

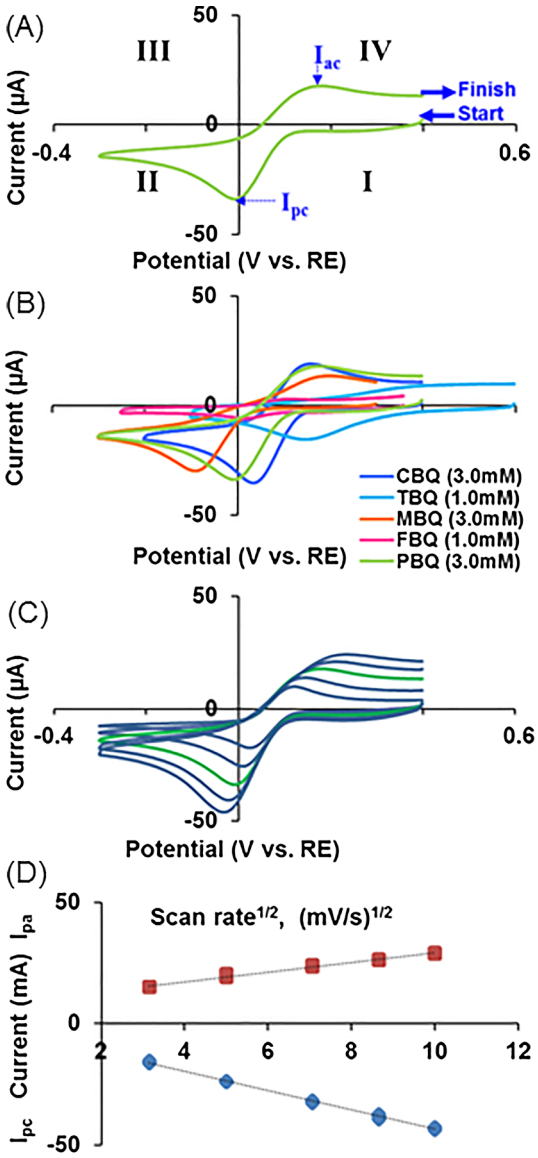

Fig. 13. (A) Cyclic voltammogram of PBQ (3.0 mM) in phosphate buffer (50. mM, pH 7.0) recorded at a scan rate of 50 mV/s, (B) Cyclic voltammograms of MBQ, FBQ, PBQ, CBQ, and TBQ in phosphate buffer (50. mM, pH 7.0) recorded at a scan rate of 50 mV/s at 3.0 mM (for MBQ, PBQ, and CBQ) or at 1.0 mM for FBQ and TBQ), (C) Cyclic voltammograms of PBQ (3.0 mM) in phosphate buffer (50. mM, pH 7.0) recorded at a scan rate of 10, 25, 50, 75, 100 mV/s, (D) I_{pc} vs. scan rate$^{1/2}$ and I_{ac} vs. scan rate$^{1/2}$.

almost 3-fold (Fig. 3B and Table 1). Table 1 shows that the anisotropy values also increased with the increase in PBQ concentration, indicating substantial structural changes to LYZ, most likely protein size increase due to oligomerization. In Fig. 8, SDS-PAGE results also show that as the PBQ concentration increases, the degree of LYZ modification intensified. For example, the dimer band appeared noticeably at 120 min for PBQ at 0.10 mM, 30 min for 0.50 mM, and 10 min for 1.0 mM, respectively. Similar PBQ-concentration dependency of protein modifications was also observed for RNase in our previous studies [26,27].

As expected, increasing the reaction temperature lead to more significant LYZ modifications. Fluorescence intensity (Fig. 5A) and the NIFI values (Table 1) decreased as incubation temperature increased from 27 °C to 42 °C. The PBQ-adduct formation, monitored by the increased absorption in the 300–400 nm range, also increased as the temperature increased from 27 °C to 42 °C (Fig. 5B). SDS-PAGE features presented in Fig. 10 show more significant LYZ modifications at higher temperature as the formation of smearing bands corresponding to polymeric aggregates occurred earlier. For the reaction at 42 °C, LYZ plaque formation was visibly recognizable especially at 24 h, resulting in less solubilization of modified LYZ for SDS-PAGE analysis (lanes 8 in Fig. 10).

Investigating LYZ modifications by PBQ at different pH conditions showed that more significant modifications occur at higher pH conditions. Fig. 9 shows that SDS-PAGE band corresponding to dimer appear at shorter incubation times at higher pH values than at lower pH conditions. Also, at higher pH conditions, formation of smearing bands corresponding to polymeric aggregates occurred earlier. For the incubation at pH 8.0, LYZ plaque formation was clearly visible especially at 24 h, resulting in less solubilization of modified LYZ for SDS-PAGE analysis (lanes 8 on Fig. 9). Fig. 4 also shows lower fluorescence intensity (Fig. 4A) and higher absorption in the 300–400 nm range (Fig. 4B) at pH 8.0 than at pH 6.0 consistent with more significant LYZ modifications at higher pH conditions. As seen in Table 1, NIFI values decreased and A_{348} increased for LYZ + PBQ as the pH of solution increases.

For the pH-dependent study of the control LYZ, the highest fluorescence intensity of unmodified LYZ in phosphate buffer was obtained at pH = 7.0, while the lowest fluorescence intensity was obtained at pH = 8.0 (Fig. 4A). The W-related fluorescence peaking feature at pH 7 for proteins, particularly focused on LYZ, was explained by the quenching effect of protonated carboxylic group (COOH) on W at the acidic pH and the quenching effect of ionized Y residue at the basic pH [41–43,51]. However, one cannot completely exclude quenching possibilities by other sources such as the local amide backbone, water, lysine, and tyrosine, possibly involving excited-state proton transfer as well as excited-state electron transfer of W [43,52–56].

The pH-dependent LYZ modifications in the presence of PBQ can be understood, considering that increasing the pH will lead to more activated amino acid residues such as lysine and arginine by shifting the equilibrium from $-NH_3^+$ group toward $-NH_2$ through deprotonation. This shifting will increase the concentration of $-NH_2$ groups which are more nucleophilic and more prone to adduct formation (Path A, Fig. 1) and lysine oxidation (Path C). If lysine oxidation is a key step leading to polymerization as well as oligomerization, a decrease in fluorescence intensity of LYZ + PBQ would be expected as pH increases. The possibility of Y residue forming unprotonated Y, therefore leading to fluorescence quenching, is less likely in the studied range of pH 6.0 to 8.0, since pK_a of OH on the phenol ring is 10.06 and the ionization of the OH is negligible in the range [57]. The UV–Vis spectra of LYZ + PBQ suggest that adduct formation amplified as pH increased from 6.0 to 8.0 based on the increase in A_{346}. Taken together with fluorescence data, the fluorescence intensity decrease for LYZ + PBQ may be due to donor–acceptor energy transfer (ET) between a covalently-bound PBQ and W in LYZ. Since ET typically occurs when there is spectral overlap between the fluorescence region of a donor and the absorption region of an acceptor [41,43], this interpretation on the fluorescence reduction is reasonable. Typically BQs including PBQ and their reduced form absorb at 280–290 nm region in addition to the visible region [26–28], which overlaps with the W fluorescence region. Once the donor W in LYZ emits energy at a shorter wavelength upon excitation, the acceptor PBQ can absorb the transferred energy, leading to non-radiative ET. In this regard, PBQ or other BQs can be included to the list of W quenchers. This finding is also consistent with the broad understanding on why W, a single fluorophore, can have such complex photo-physics with multiple fluorescence lifetimes or diverse fluorescence behavior that can be affected by slight changes in the surrounding environment.

Another aspect investigated by fluorescence and UV–Vis spectroscopy was the LYZ modification at various incubation time intervals. This time-lapse fluorescent study for LYZ + PBQ revealed that the NIFI values for control LYZ changed from 100 for LYZ subjected to reaction conditions except the presence of PBQ (*i.e.*, incubation for 24 h at 37 °C and hourly irradiation scans) to 109 for the LYZ subjected directly to

dialysis. This decrease of a NIFI value by 9 upon 24-h incubation is most likely due to photo-damage caused by hourly irradiation of LYZ, even in the absence of PBQ. In addition, the other time-lapse NIFI values for LYZ + PBQ exhibited an interesting feature with an initial increase in NIFI for 1 h and 2 h of incubation followed by slight decrease for 3 h and a significant decrease for 24 h exposure to PBQ. The slight increase in fluorescence intensity for LYZ + PBQ at early stages of reaction (1 or 2 h exposure to PBQ) in comparison to control LYZ (either at 0 h or 24 h incubation) is probably due to creation of modified protein species with higher fluorescence intensity most likely through adduct formation or crosslinking. The adduct-formation stage of protein modification involves the covalently bonding of one PBQ molecule to the protein. Through redox cycling this attached PBQ can be transformed into hydroquinone (HQ), which is fluorescent unlike PBQ. Therefore, the increase in fluorescence emission may be due to the presence of fluorescent HQs that are covalently linked to LYZ. It is also possible that the early stages of protein modification (*i.e.*, the adduct formation or dimerization) is accompanied by conformational changes of LYZ leading to increase quantum yield and therefore increased fluorescence intensity. The monitoring of LYZ + PBQ reaction mixtures show sometimes an increase fluorescence intensity upon hourly fluorescence scans but these mixtures also contain unreacted PBQ, fluorescent HQ species formed by reduction of PBQ, and other small molecules that may interfere with the protein fluorescence. The increase of fluorescence intensity for a reaction mixture cannot be undoubtedly assigned to the protein modification until dialysis is performed and the interfering small molecules are removed, as it was done in this study. It is interesting to point out that these protein modifications in initial stages although are accompanied by an increase fluorescence intensity, they are not associated with an increase in the absorbance at 346 nm in the UV–Vis spectra. As shown in Fig. 6B, time-dependent UV–Vis spectra showed that there is no significant absorption in the 300–400 nm region within two hours of incubation when LYZ was reacted with PBQ at various incubation times. This study suggests that PBQ-adduct formation at detectable levels take as long as 3 h under the diluted conditions used here. However, the 24 h-scan clearly shows adduct formation, with the A_{346} value of 0.09.

Another challenge while investigating the LYZ modifications by BQs was the plaque formation under harsh conditions which disrupted monitoring LYZ modifications using fluorescence and UV–Vis spectroscopy. As shown in Fig. 14, when both LYZ (0.050 mM) and RNase (0.050 mM) were reacted with PBQ (1.5 mM), both LYZ + PBQ and RNase + PBQ started as colorless solutions at time 0 h (Fig. 14A). As time progressed, the color of both reactions changed into orange while LYZ + PBQ exhibited opaque orange color as early as 2 h (see Supplementary Material). At 24 h, LYZ plaque formation was clearly visible with crystalline-like aggregates for LYZ + PBQ, while RNase + PBQ exhibited transparent dark reddish brown color (Fig. 14B/C). The amyloidal plaques for LYZ + PBQ were sticking to the cuvette surface (Fig. 14C, cuvette on the left), while the emptied cuvette for RNase + PBQ (Fig. 14C, cuvette on the right) at 24 exhibited clear surface. In order to clean the LYZ + PBQ cuvette, it had to be treated with concentrated HNO_3 for 48 h.

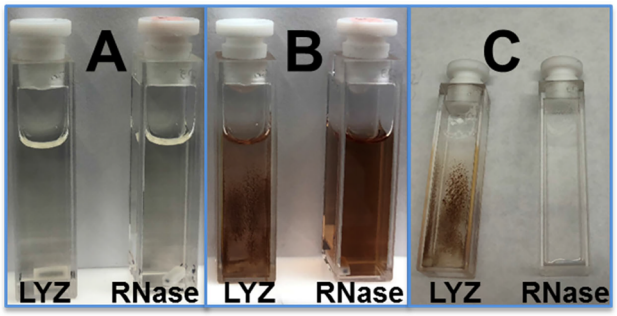

Fig. 14. Reactions of LYZ + PBQ (Left cuvette) vs. RNase + PBQ (Right cuvette). All reactions were carried out by incubating each protein (0.050 mM) treated with PBQ (1.5 mM) in phosphate buffer (50. mM, pH 7.0) at 37 °C. (A) Reactions at 0 h, (B) reactions at 24 h, (C) Emptied cuvettes after 24 h incubation.

LYZ used in this study has a MM of 14,388 Da, 147 amino acid residues, and pI value of 11.0 [58–60]. RNase used in the previous studies has a similar MM value of 13,682 Da, 124 amino acid residues, and a pI value of 9.4 [60,61]. The number of lysine, serine, threonine, and cysteine, respectively, are 6, 9, 7, and 8 for LYZ and 10, 15, 10, and 8 for RNase. LYZ has 4 tyrosine and 7 tryptophan, while RNase has 6 tyrosine and 0 tryptophan. Considering the similarity between LYZ and RNase in terms of MM, pI values, and types of amino acid residues each contains, it is interesting to observe such vast outcomes under treatment with PBQ, with LYZ leading to formation of insoluble plaques under high PBQ concentrations. In order to circumvent plaque formation, more diluted LYZ solutions were used for studying fluorescence behavior of LYZ in the presence of BQs.

To compare modifications of LYZ and RNase under same reaction conditions using fluorescence and UV–Vis spectroscopy, we carried out reactions of RNase (0.010 mM) with PBQ at three different concentrations (0.010 mM, 0.050 mM and 0.10 mM, respectively) in a phosphate buffer (50. mM, pH 7.0) for 24 h at 37 °C (see Supplementary Material). Compared to a NIFI of 100 for the protein with no PBQ, the NIFI values of 71, 43, and 35 for LYZ were smaller than the NIFI values of 86, 64, and 49 obtained for RNase at PBQ concentrations of 0.010 mM, 0.050 mM and 0.10 mM, respectively. A_{346} values for RNase were also greater that the values for LYZ implying more significant modifications for LYZ than RNase under same reaction conditions, even in the absence of plaque formation.

In order to better understand LYZ modifications from a structural standpoint, we rendered LYZ structure using DeepView-SwissPDB Viewer (Fig. 11). As shown in the proposed mechanism (Fig. 1), lysine oxidation in LYZ is expected to serve a key role in oligomerization and polymerization of LYZ through protein cross-linking. Therefore, we examined the locations of all lysine residues (residues 1, 13, 33, 96, 97, and 116, respectively) in LYZ. Previously published reports regarding the positions of W residues are consistent with our rendered model of LYZ (PDB ID: 5K2K), revealing three W residues (W62, W63, W108) located at the binding site for LYZ substrates, with two of the W residues buried in the hydrophobic pocket (W108, W111) while W123 distanced from other W residues [30–32]. It is known that the LYZ fluorescence predominantly relies on W62 (more exposed with SA value of 3) and W108 (less exposed with SA value of 1). W62 is generally viewed as a major contributor although this is still debated [30,62], while the fluorescence contribution from other W residues well as Y residues was found trivial [30,31]. Regarding, Föster energy transfer (FET) possibility, Y-to-W energy transfer was suggested insignificant [63], while a direct, non-radiative, homo-tryptophanyl transfer was strongly suggested from the donor W108 to the acceptor W62 [30,31]. The idea of inter-tryptophanyl energy transfer through W63 was not supported based on fluorescence lifetime experiments upon varying pH, and this might be due to less interaction between W62 and W63 as both residues are exposed to solvent [30,31]. With LYZ fluorescence relying mostly on W62, it is expected to see greater decrease in fluorescence intensity for LYZ than other proteins under similar conditions. Indeed, the decrease in LYZ fluorescence intensity was more significant compared to that of RNase in similar conditions.

Separately, the I-TASSER SA profile of lysine residues in LYZ suggests that quinones can easily oxidize lysine 1 and 116 into oxo-lysine and probably convert other lysine residues as well as soon as there is a conformational change in LYZ. Then, the formed oxo-lysine can react with an unmodified lysine from other LYZ resulting in crosslinking and this hypothesis is confirmed by our observation on SDS-PAGE. The

oxidation of lysine playing a critical role becomes apparent as seen in the pH varying incubations monitored both at SDS-PAGE as well as fluorescence studies.

5. Conclusions

In the present study, we evidenced LYZ modification caused by a series of BQs and evaluated BQ substituent effects in protein modifications. Our findings suggest that BQ substituent effects plays a role in LYZ modification, with CBQ and TBQ being more efficient, while MBQ and FBQ being less efficient in LYZ modification. This efficiency rank order of MBQ < FBQ < PBQ < CBQ < TBQ was in good agreement with the trend in reduction potentials of BQs. In addition, we found out variation in pH, temperature, and PBQ concentrations affected the degree of LYZ modification, with more LYZ modification occurring in higher pH, temperature, and PBQ concentrations. Comparatively to RNase, LYZ modification was more complex accompanying adduct formation, oligomerization, polymerization, and plaque formation.

Acknowledgment

The study was supported in part by Grote Fund, Wheeler Fund, UC Foundation Fund, and PSRA awards at the University of Tennessee at Chattanooga, United States (UTC). The authors are thankful to the analytical chemistry faculty at UTC for their support on using Wavenow software.

Conflict of interest

The authors declare that there are no conflicts of interests.

Appendix A. Supplementary material

Supplementary data to this article can be found online at https://doi.org/10.1016/j.bioorg.2019.01.018.

References

[1] J.M. Berg, J.L. Tymoczko, L. Stryer, Biochemistry, sixth ed., W. H. Freeman and Co., New York, 2006.
[2] C.M. Dobson, Protein folding and misfolding, Nature 426 (2003) 884–890.
[3] C.M. Dobson, Protein misfolding, evolution and disease, Trends Biochem. Sci. 24 (1999) 329–332.
[4] P. Tompa, Intrinsically disordered proteins: a 10-year recap, Trends Biochem. Sci. 37 (2012) 509–516.
[5] M. Stefani, Protein misfolding and aggregation: new examples in medicine and biology of the dark side of the protein world, Biochim. Biophys. Acta-Mol. Basis Dis. 1739 (2004) 5–25.
[6] J.N. Onuchic, P.G. Wolynes, Z. Lutheyschulten, N.D. Socci, Toward an outline of the topography of a realistic protein-folding funnel, PNAS 92 (1995) 3626–3630.
[7] J.D. Bryngelson, J.N. Onuchic, N.D. Socci, P.G. Wolynes, Funnels, pathways, and the energy landscape of protein-folding – a synthesis, Prot.-Struct. Funct. Genet. 21 (1995) 167–195.
[8] T. Borwankar, C. Rothlein, G. Zhang, A. Techen, C. Dosche, Z. Ignatova, Natural osmolytes remodel the aggregation pathway of mutant huntingtin exon 1, Biochemistry-Us 50 (2011) 2048–2060.
[9] G. Calloni, C. Lendel, S. Campioni, S. Giannini, A. Gliozzi, A. Relini, M. Vendruscolo, C.M. Dobson, X. Salvatella, F. Chiti, Structure and dynamics of a partially folded protein are decoupled from its mechanism of aggregation, J. Am. Chem. Soc. 130 (2008) 13040–13050.
[10] J. Juarez, S.G. Lopez, A. Cambon, P. Taboada, V. Mosquera, Influence of electrostatic interactions on the fibrillation process of human serum albumin, J. Phys. Chem. B 113 (2009) 10521–10529.
[11] T.N. Niraula, K. Haraoka, Y. Ando, H. Li, H. Yamada, K. Akasaka, Decreased thermodynamic stability as a crucial factor for familial amyloidotic polyneuropathy, J. Mol. Biol. 320 (2002) 333–342.
[12] T.N. Niraula, T. Konno, H. Li, H. Yamada, K. Akasaka, H. Tachibana, Pressure-dissociable reversible assembly of intrinsically denatured lysozyme is a precursor for amyloid fibrils, Proc. Natl. Acad. Sci. U S A 101 (2004) 4089–4093.
[13] P. Pal, M. Mahato, T. Kamilya, B. Tah, R. Sarkar, G.B. Talapatra, Fibrillation of egg white ovalbumin: a pathway via biomineralization, J. Phys. Chem. B 115 (2011) 4259–4265.
[14] A.L. Horwich, G.W. Farr, W.A. Fenton, GroEL-GroES-mediated protein folding, Chem. Rev. 106 (2006) 1917–1930.
[15] M. Hochstrasser, Introduction to intracellular protein degradation, Chem. Rev. 109 (2009) 1479–1480.
[16] A.J. Marques, R. Palanimurugan, A.C. Matias, P.C. Ramos, R.J. Dohmen, Catalytic mechanism and assembly of the proteasome, Chem. Rev. 109 (2009) 1509–1536.
[17] F. Chiti, C.M. Dobson, Protein misfolding, functional amyloid, and human disease, Annu. Rev. Biochem. 75 (2006) 333–366.
[18] F. Chiti, C.M. Dobson, Amyloid formation by globular proteins under native conditions, Nat. Chem. Biol. 5 (2009) 15–22.
[19] P.T. Sattianayagam, S.D. Gibbs, D. Rowczenio, J.H. Pinney, A.D. Wechalekar, J.A. Gilbertson, P.N. Hawkins, H.J. Lachmann, J.D. Gillmore, Hereditary lysozyme amyloidosis – phenotypic heterogeneity and the role of solid organ transplantation, J. Intern. Med. 272 (2012) 36–44.
[20] M. Andreasen, N. Lorenzen, D. Otzen, Interactions between misfolded protein oligomers and membranes: a central topic in neurodegenerative diseases? Biochim. Biophys. Acta-Biomembr. 1848 (2015) 1897–1907.
[21] A. Dhulesia, N. Cremades, J.R. Kumita, S.T. Hsu, M.F. Mossuto, M. Dumoulin, D. Nietlispach, M. Akke, X. Salvatella, C.M. Dobson, Local cooperativity in an amyloidogenic state of human lysozyme observed at atomic resolution, J. Am. Chem. Soc. 132 (2010) 15580–15588.
[22] J. Kim, Biological implications of benzoquinones, Quinone: Occurrence, Medicinal Uses and Physiological Importance, Nova Science Publisher Inc, 2013.
[23] J.L. Bolton, M.A. Trush, T.M. Penning, G. Dryhurst, T.J. Monks, Role of quinones in toxicology, Chem. Res. Toxicol. 13 (2000) 135–160.
[24] J. Kim, I.N. Lee, Inactivation of bovine plasma amine oxidase by 1,1,1-trihalo-3-aminopropanes, Bioorg. Chem. 75 (2017) 265–273.
[25] J. Kim, Y.M. Zhang, C.Z. Ran, L.M. Sayre, Inactivation of bovine plasma amine oxidase by haloallylamines, Bioorg. Med. Chem. 14 (2006) 1444–1453.
[26] J. Kim, T.V. Albu, A.R. Vaughn, S.M. Kang, E.A. Carver, D.M. Stickle, A comparison study on ribonuclease A modifications induced by substituted p-benzoquinones, Bioorg. Chem. 59 (2015) 106–116.
[27] J. Kim, A.R. Vaughn, C. Cho, T.V. Albu, E.A. Carver, Modifications of ribonuclease A induced by p-benzoquinone, Bioorg. Chem. 40 (2012) 92–98.
[28] A.R. Vaughn, C.B. Redman, S.M. Kang, J. Kim, Biological implications of 2-chlorocyclohexa-2,5-diene-1,4-dione toward ribonuclease A, Adv. Biosci. Biotech. 4 (2013) 22–28.
[29] N. Gregersen, P. Bross, S. Vang, J.H. Christensen, Protein misfolding and human disease, Annu. Rev. Genomics Hum. Genet. 7 (2006) 103–124.
[30] C. Formoso, L.S. Forster, Tryptophan fluorescence lifetimes in lysozyme, J. Biol. Chem. 250 (1975) 3738–3745.
[31] T. Imoto, J.A. Rupley, F. Tanaka, L.S. Forster, Fluorescence of lysozyme – emissions from tryptophan residues 62 and 108 and energy migration, PNAS 69 (1972) 1151–2000.
[32] S. Yamashita, E. Nishimoto, A.G. Szabo, N. Yamasaki, Steady-state and time-resolved fluorescence studies on the ligand-induced conformational change in an active lysozyme derivative, Kyn62-lysozyme, Biochemistry-Us 35 (1996) 531–537.
[33] M. Dumoulin, J.R. Kumita, C.M. Dobson, Normal and aberrant biological self-assembly: insights from studies of human lysozyme and its amyloidogenic variants, Acc. Chem. Res. 39 (2006) 603–610.
[34] A.C. Hamill, S.C. Wang, C.T. Lee, Probing lysozyme conformation with light reveals a new folding intermediate, Biochemistry-Us 44 (2005) 15139–15149.
[35] A.K. Buell, A. Dhulesia, M.F. Mossuto, N. Cremades, J.R. Kumita, M. Dumoulin, M.E. Welland, T.P.J. Knowles, X. Salvatella, C.M. Dobson, Population of nonnative states of lysozyme variants drives amyloid fibril formation, J. Am. Chem. Soc. 133 (2011) 7737–7743.
[36] U.K. Laemmli, Cleavage of structural proteins during the assembly of the head of bacteriophage T4, Nature 227 (1970) 680–685.
[37] K. Weber, M. Osborn, The reliability of molecular weight determinations by dodecyl sulfate polyacrylamide gel electrophoresis, J. Biol. Chem. 244 (1969) 4406–4412.
[38] A. Bairoch, R. Apweiler, The SWISS-PROT protein sequence database and its supplement TrEMBL in 2000, Nucl. Acids Res 28 (2000) 45–48.
[39] http://www.expasy.ch/spdbv/.
[40] Y. Zhang, I-TASSER server for protein 3D structure prediction, BMC Bioinf. 9 (2008) 40.
[41] S.S. Lehrer, G.D. Fasman, Fluorescence of lysozyme and lysozyme substrate complexes – separation of tryptophan contributions by fluorescence difference methods, J. Biol. Chem. 242 (1967) 4644–5000.
[42] S.S. Lehrer, G.D. Fasman, The fluorescence of lysozyme and lysozyme substrate complexes, Biochem. Biophys. Res. Commun. 23 (1966) 133–138.
[43] J.R. Lakowicz, Principles of Fluorescence Spectroscopy, third ed., Springer, New York, NY, 2006.
[44] F. Scholz, Electroanalytical Methods: Guide to experiments and applications, 2nd ed.,, Springer, 2015.
[45] G.A. Mabbott, An introduction to cyclic voltammetry, J. Chem. Educ. 60 (1983) 697–702.
[46] M. Quan, D. Sanchez, M.F. Wasylkiw, D.K. Smith, Voltammetry of quinones in unbuffered aqueous solution: Reassessing the roles of proton transfer and hydrogen bonding in the aqueous Electrochemistry of Quinones, J. Am. Chem. Soc. 129 (2007) 12847–12856.
[47] G. Macfie, R.G. Compton, Characterisation of the sonicated ring-pellet reactor and sono-ring-disc electrodes, J. Electroanal. Chem. 503 (2001) 125–132.
[48] M. Sato, K. Murakami, M. Uno, Y. Nakagawa, S. Katayama, K. Akagi, Y. Masuda, K. Takegoshi, K. Irie, Site-specific inhibitory mechanism for amyloid beta42 aggregation by catechol-type flavonoids targeting the Lys residues, J. Biol. Chem. 288 (2013) 23212–23224.
[49] P. Velander, L. Wu, W.K. Ray, R.F. Helm, B. Xu, Amylin amyloid inhibition by

flavonoid baicalein: key roles of its vicinal dihydroxyl groups of the catechol moiety, Biochemistry-Us 55 (2016) 4255–4258.
[50] S. Feng, X.H. Song, C.M. Zeng, Inhibition of amyloid fibrillation of lysozyme by phenolic compounds involves quinoprotein formation, FEBS Lett. 586 (2012) 3951–3955.
[51] D.R. James, W.R. Ware, Multiexponential fluorescence decay of indole-3-alkanoic acids, J. Phys. Chem. 89 (1985) 5450–5458.
[52] Y. Chen, M.D. Barkley, Toward understanding tryptophan fluorescence in proteins, Biochemistry-Us 37 (1998) 9976–9982.
[53] E. Vanderdonckt, Fluorescence solvent shifts excited state Pks of indole derivatives, Bull. Soc. Chim. Belg. 78 (1969) 69-+.
[54] R.W. Ricci, J.M. Nesta, Intermolecular and intramolecular quenching of indole fluorescence by carbonyl-compounds, J. Phys. Chem. 80 (1976) 974–980.
[55] R.W. Ricci, Determination of activation-energy of a non-radiative decay manifold – physical-chemistry experiment, J. Chem. Educ. 51 (1974) 692–694.
[56] R.W. Ricci, K.B. Kilichow, Fluorescence quenching of indole ring-system by lanthanide ions, J. Phys. Chem. 78 (1974) 1953–1956.
[57] P.A. Dewick, Essentials of Organic Chemistry: For Students of Pharmacy, Medicinal Chemistry and Biological Chemistry, John Wiley & Sons Ltd., 2006.
[58] R.H.C. Strang, Purification of egg-white lysozyme by ion-exchange chromatography, Biochem. Educ. 12 (1984) 57–59.
[59] K. Harata, T. Akiba, Phase transition of triclinic hen egg-white lysozyme crystal associated with sodium binding, Acta Crystallogr. Sect. D-Biol. Crystallogr. 60 (2004) 630–637.
[60] V.N. Uversky, A.L. Fink, Protein Reviews: Protein Misfolding, Aggregation, and Conformational Diseases vol. 6, (2007).
[61] R.T. Raines, Ribonuclease A, Chem. Rev. 98 (1998) 1045–1065.
[62] G.Y. Yashinsky, Fluorescence decay of lysozyme and of iodine oxidized lysozyme, FEBS Lett. 26 (1972) 123–126.
[63] M.J. Kronman, L.G. Holmes, The fluorescence of native, denatured and reduced-denatured proteins, Photochem. Photobiol. 14 (1971) 113–134.